CHEMISTRY OF MATERIALS
Article

Chem. Mater. **2010,** *22,* 2857–2863 2857
DOI:10.1021/cm100071z

Solution-Combustion Synthesized Nanocrystalline $Li_4Ti_5O_{12}$ As High-Rate Performance Li-Ion Battery Anode

A. S. Prakash,[†] P. Manikandan,[†] K. Ramesha,[†] M. Sathiya,[†] J-M. Tarascon,[‡,∥] and A. K. Shukla*[,§]

[†]*Central Electrochemical Research Institute-Chennai Unit, CSIR-Madras Complex, Chennai-600 113, India,* [‡]*Materials Department, University of California Santa Barbara, Santa Barbara, California 93106, and* [§]*Solid State and Structural Chemistry Unit, Indian Institute of Science, Bangalore-560 012, India.* [∥]*Current address: Laboratoire de Réactivité et Chimie des Solides, Université de Picardie Jules Verne, CNRS UMR 6007, 33 rue Saint Leu, 80039, Amiens, France.*

Received January 8, 2010. Revised Manuscript Received March 10, 2010

Nanocrystalline $Li_4Ti_5O_{12}$ (LTO) crystallizing in cubic spinel-phase has been synthesized by single-step-solution-combustion method in less than one minute. LTO particles thus synthesized are flaky and highly porous in nature with a surface area of 12 m^2/g. Transmission electron micrographs indicate the primary particles to be agglomerated crystallites of varying size between 20 and 50 nm with a 3-dimensional interconnected porous network. During their galvanostatic charge−discharge at varying rates, LTO electrodes yield a capacity value close to the theoretical value of 175 mA h/g at C/2 rate. The electrodes also exhibit promising capacity retention with little capacity loss over 100 cycles at varying discharge rates together with attractive discharge-rate capabilities yielding capacity values of 140 mA h/g and 70 mA h/g at 10 and 100 C discharge rates, respectively. The ameliorated electrode-performance is ascribed to nano and highly porous morphology of the electrodes that provide short diffusion-paths for Li in conjunction with electrolyte percolation through the electrode pores ensuring a high flux of Li.

Introduction

The pressing need to switch over to electric cars in the future necessitates developing lithium batteries that far exceed the current technology. In this context, high-performance anode and cathode materials for the lithium batteries would be most desirable. Nanocrystalline $Li_4Ti_5O_{12}$ (LTO) is an attractive anode material for Li-ion batteries[1,2] for electric vehicles as (a) it is cheaper, (b) it experiences zero-strain during lithium intercalation/deintercalation,[3−5] (c) it has the unique feature of lithium intercalation/deintercalation with little change in the unit-cell volume,[3,4] (d) it offers a convenient voltage-plateau at 1.5 V versus Li^+/Li compatible with polymer electrolytes and high-voltage cathodes;[6] the voltage plateau happens to be much above the reduction potential of most organic electrolytes mitigating the formation of solid-electrolyte interface (SEI),[7,8] (e) it exhibits little irreversible capacity,[1,3,5] (f) it shows excellent cycling performance with long cycle life,[1,3,5] (g) it has high enough operating voltage-plateau that avoids formation of lithium dendrites making the battery safer.[5,9] The only disadvantage of LTO is its poor electronic conductivity that limits its full capacity at high charge−discharge rates.[9]

In the literature,[10,11] effort has been expended to increase the electronic conductivity of LTO by (a) doping, (b) its nitridation to form oxynitride species on its surface,[12] and (c) carbon coating of LTO particles.[13] The increase in electronic conductivity of LTO has facilitated higher-rate operability of LTO anodes so that $LiMn_2O_4$/$Li_4Ti_5O_{12}$ ion cells are on the verge of being commercialized. It is also well-known that shorter diffusion-lengths for Li^+-ions and electronic transport in nanoparticles improve the high-rate performance of lithium battery anodes.[14]

*To whom correspondence should be addressed. Phone: +91-80-22932795. Fax: +91-80-23601310. E-mail: shukla@sscu.iisc.ernet.in.

(1) Ariyoshi, K.; Ohzuku, T. *J. Power Sources*. **2007**, *174*, 1258.
(2) Jansen, A. N.; Kahaian, A. J.; Kepler, K. D.; Nelson, P. A.; Amine, K.; Dees, D. W.; Vissers, D. R.; Thackeray, M. M. *J. Power Sources*. **1999**, *81−82*, 902.
(3) Ohzuku, T.; Ueda, A.; Yamamoto, N. *J. Electrochem. Soc*. **1995**, *142*, 1431.
(4) Scharner, S.; Weppner, W.; Schmid-Beurmann, P. *J. Electrochem. Soc*. **1999**, *146*, 857.
(5) Zaghib, K.; Simoneau, M.; Armand, M.; Gauthier, M. *J. Power Sources* **1999**, *81/82*, 300.
(6) Prosini, P. P.; Mancini, R.; Petrucci, L. *Solid State Ionics* **2001**, *144*, 185.
(7) Aricò, A. S.; Bruce, P.; Scrosati, B.; Tarascon, J.-M.; Schalkwijk, W. V. *Nat. Mater*. **2005**, *4*, 366.
(8) Huang, S. H.; Wen, Z. Y.; Zhang, J. C.; Gu, Z. H.; Xu, X. H. *Solid State Ionics* **2006**, *177*, 851.
(9) Yang, Z.; Choi, D.; Kerisit, S.; Rosso, K. M.; Wang, D.; Zhang, J.; Graff, G.; Liu, J. *J. Power Sources* **2009**, *192*, 588.
(10) Chen, C. H.; Vaughey, J. T.; Jansen, A. N.; Dees, D. W.; Kahaian, A. J.; Goacher, T; Thackeray, M. M. *J. Electrochem. Soc*. **2001**, *148* (1), A102.
(11) Robertson, A. D.; Trevino, L.; Tukamoto, H.; Irvine, J. T. S. *J. Power Sources*. **1999**, *81−82*, 352.
(12) Park, K.-S.; Benayad, A.; Kang, D.-J.; Doo, S.-G. *J. Am. Chem. Soc*. **2008**, *130*, 14930.
(13) Cheng, L.; Li, X.-L.; Liu, H.-J.; Xiong, H-M; Zhang, P.-W.; Xia, Y.-Y. *J. Electrochem. Soc*. **2007**, *154*, A692.
(14) Bruce, P. G.; Scrosati, B.; Tarascon, J.-M. *Angew. Chem., Int. Ed*. **2008**, *47*, 2930.

Published on Web 03/30/2010

To this end, much effort has been made to synthesize nanostructured LTO with varying morphologies and particle size, and their electrochemical performance studied. For example, Li et al.[15] have shown improved performance with one-dimensional (1D) LTO nanostructures, namely, nanotubes/nanowires synthesized by hydrothermal method. Tang et al.[16] have reported nanosheets of flower like LTO synthesized by a hydrothermal route in the presence of glycol solution that delivers high capacity even at very high charge−discharge rates. Sorensen et al.[17] have reported 3D-ordered macroporous LTO with thin wall thickness which could deliver excellent high-rate capacities. Jiang et al.[18] have reported the synthesis of hollow spheres of LTO by a sol−gel method using carbon spheres as templates that exhibit high-rate performance. Furthermore, nanoparticles of LTO have also been realized by spray pyrolysis,[19] combustion,[20−22] as well as other decomposition techniques.[23,24]

Combustion or solution-combustion synthesis is a well-known method for the preparation of nanocrystalline oxides.[25−28] The method, involving redox reaction between oxidizer and a fuel, is simple, instantaneous, and cost-effective. The method yields nanosized material almost instantaneously and can be used to prepare a variety of complex oxides in nanocrystalline form.[25,26,29,30] Yuan et al.[20,21] have reported the synthesis of nano LTO powders by combustion synthesis with combustion reaction initiated at < 250 °C. The combustion product in this case happens to be partially formed LTO with anatase and rutile TiO_2 impurities requiring further thermal treatment of the combustion product at temperatures > 800 °C for about 5 h to obtain single-phased LTO. By contrast, the method reported in this study is different and helps in realizing single-phased LTO directly from the combustion reaction of metal nitrates-glycine initiated at about 800 °C; LTO thus synthesized is nanocrystalline with high porosity and exhibits superior rate-performance compared to LTO prepared from the methods reported earlier.

Experimental Section

LTO nanopowders were prepared by solution-combustion synthesis using titanyl nitrate [$TiO(NO_3)_2$] and $LiNO_3$ as the oxidant precursors and glycine as the fuel. The aqueous solution of titanyl nitrate [$TiO(NO_3)_2$] was obtained a priori by reacting 1:1 nitric acid with titanyl hydroxide [TiO-$(OH)_2$] which was obtained by the hydrolysis of titanium isopropoxide [Ti(*i*-$OPr)_4$] at < 10 °C with dilute ammonia followed by filtration and washing. Ti-ion concentration in the solution was estimated by the colorimetric method in the presence of H_2O_2 and H_2SO_4.[31]

In a typical preparation, an aqueous redox mixture containing stoichiometric amount of titanyl nitrate (0.0362 mol), 2 g of $LiNO_3$ (0.0289 mol), and 4.22 g of glycine (0.0562 mol) were taken in a 120 mL alumina crucible and placed into a muffle furnace preheated to 800 °C. The stoichiometry of metal nitrate to glycine is calculated assuming the complete combustion to yield corresponding oxide product and CO_2, N_2, and H_2O as byproducts.[25] In the furnace, the solution boils and water evaporates followed by frothing, and bursts into combustion with white incandescent light. The reaction completes in a few seconds. The reaction crucible was then removed from the furnace and allowed to cool. The froth-like voluminous powder was crushed with mortar and pestle, and stored for further studies.

X-ray diffraction (XRD) patterns for the LTO samples thus prepared were recorded using an X'pert PRO-PANalytical Diffractometer using CuK_α radiation. The morphology of the powder samples was studied using a Scanning Electron Microscope (JEOL 5600LV). Transmission Electron microscopy studies of the samples were conducted using a Technai 20 Transmission Electron Microscope operated at 200 kV. Chemical analyses of the samples were carried out using a Perkin-Elmer Atomic Absorption Spectrometer. The surface area for powdered samples is measured by the Brunauer−Emmett−Teller (BET) method using a Surface Area Analyzer (Belsorp Japan). Sample porosity was extracted using the Barrett−Joyner−Halenda (BJH) method. Electrochemical characterizations were performed using CR2032 coin-type cells. The positive electrode material was prepared by blending a ball-milled mixture of 80% active material and 15% SP carbon with 5% poly(vinylidene fluoride) dissolved in *N*-methyl-2-pyrrolidone. The electrode slurry thus obtained was coated over stainless steel discs and dried overnight under vacuum at 80 °C. The weight of active material was ~ 4 mg/cm^2. The cells were assembled and sealed in an argon-filled glovebox with lithium foil as the anode and 1 M $LiPF_6$ dissolved in EC/DMC (1:1 by volume) as the electrolyte. The cells thus fabricated were cycled galvanostatically in the voltage range between 1 V and 2 V versus lithium using VMP3Z (Biologica) Multi-Channel Potentiostat/Galvanostat.

Results and Discussion

The solution−combustion method reported here is simple, rapid, and environmentally benign, and is different

(15) Li, J. R.; Tang, Z. L.; Zhang, Z. T. *Electrochem. Commun.* **2005**, *7*, 894.
(16) Tang, Y. F.; Yang, L.; Qiu, Z.; Huang, J. S. *Eectrochem. Commun.* **2008**, *10*, 1513.
(17) Sorensen, E. M.; Barry, S. J.; Jung, H. K.; Rondinelli, J. R.; Vaughey, J. T.; Poeppelmeier, K. R. *Chem. Mater.* **2006**, *18*, 482.
(18) Jiang, C.; Zhou, Y.; Honma, I.; Kudo, T.; Zhou, H. *J. Power Sources.* **2007**, *166*, 514.
(19) Ju, S. H.; Kang, Y. C. *J. Power Sources.* **2009**, *189*, 185.
(20) Yuan, T.; Cai, R.; Wang, K.; Ran, R.; Liu, S.; Shao, Z. *Ceram. Int.* **2009**, *35*, 1757.
(21) Yuan, T.; Wang, K.; Cai, R.; Ran, R.; Shao, Z. *J. Alloys. Compd.* **2009**, *477*, 665.
(22) Raja, M. W.; Mahanty, S.; Kundu, M.; Basu, R. N. *J. Alloys. Compd.* **2009**, *468*, 258.
(23) Hao, Y.-J.; Lai, Q.-Y.; Lu, J.-Z.; Liu, Q.-D.; Ji, X.-Y. *J. Alloys. Compd.* **2007**, *439*, 330.
(24) Hao, Y.-J.; Lai, Q.-Y.; Lu, J.-Z.; Wang, H.-L.; Chen, Y.-D.; Ji, X.-Y. *J. Power Sources.* **2006**, *158*, 1358.
(25) Patil, K. C.; Hegde, M. S.; Tanu, R.; Aruna, S. T. *Chemistry of nanocrystalline oxide materials; combustion synthesis, properties and applications*; World Scientific: Singapore, 2008.
(26) Prakash, A. S.; Khadar, A. M. A.; Patil, K. C.; Hegde, M. S. *J. Mater. Syn. Process.* **2002**, *10*, 135.
(27) Manjunath, B.; Shivakumara, C.; Baidya, T.; Prakash, A. S.; Vasanthacharya, N. Y.; Hegde, M. S. *Mater. Res. Bull.* **2008**, *43*, 2658.
(28) Prakash, A. S.; Shivakumar, C.; Hegde, M. S. *Mater. Sci. Eng., B* **2007**, *139*, 55.
(29) Aruna, S. T.; Kini, N. S.; Rajam, N. S. *Mater. Res. Bull.* **2009**, *44*, 728.
(30) Patil, K. C.; Aruna, S. T.; Ekambaram, S. *Curr. Opin. Solid State Mater. Sci.* **1997**, *2*, 158.
(31) Vogel, A. I. A *Textbook of Quantitative Inorganic Analysis*, 5th ed.; Longman: New York, Reprint 1997; p 696.

Figure 1. Voluminous $Li_4Ti_5O_{12}$ formed after the combustion of corresponding metal nitrates with glycine at 800 °C.

from other synthetic methods, namely, nitrates decomposition, sol−gel, and so forth, which are known to release toxic gases. By contrast, during complete-combustion reaction, that is, with oxidizer/fuel ratio of 1, only CO_2, N_2, and H_2O are reported to evolve.[26] Concomitant formation of product phase along with evolution of large volumes of gases during combustion results in a highly voluminous product. Figure 1 shows the product formed after the combustion of aqueous nitrates of Li and Ti with Glycine fuel. It is found that 3.32 g of the formed product resides in about 120 cc volume. The product is highly voluminous with a tap density measured after grinding as low as 2.27 g/cm^3 against theoretical density of 3.73 g/cm^3. The averaged surface area of the powder sample as measured using the BET technique is ~12 m^2/g; the averaged pore volume observed for the sample using the BJH method is $\sim 9 \times 10^{-2}$ cm^3/g. However, the macroporosity could not be measured because of the limitation of the technique; macropores are too large to observe by N_2 adsorption method.

Figure 2 shows powder XRD patterns for the combustion products at varying temperatures. XRD patterns for the phases formed by the combustion of reactant nitrates < 800 °C are shown in Figure 2 (a) and 2(b). These XRD patterns comprise Li_2TiO_3 along with anatase and rutile forms of TiO_2. The most intense reflection for anatase at $2\theta = 25.3°$ is denoted as (*) and that for rutile at $2\theta = 27.5°$ is denoted as (#). The diffraction pattern comprise broad peaks indicating the nanocrystalline nature of the products. The broad peaks make it difficult to distinguish between Li_2TiO_3 and $Li_4Ti_5O_{12}$ phases as their diffraction peaks overlap each other. But, the diffraction peaks at $2\theta = 20.4°$ and 22.2° are specific to Li_2TiO_3 and are absent for $Li_4Ti_5O_{12}$. However, these peaks are smeared because of the low crystallinity of the material, with less than 8% intensity, causing difficulty in phase identification between Li_2TiO_3 and $Li_4Ti_5O_{12}$. Furthermore, the absence of any other peaks corresponding to lithium salts and the presence of sufficient quantity of TiO_2 impurities indicate the product to be Li_2TiO_3, a low-temperature phase pertaining to the Li−Ti−O system. The diffraction pattern of the product formed at 600 °C (not shown in Figure.2) primarily comprises Li_2TiO_3, anatase, and rutile forms of TiO_2 while the XRD pattern for the product

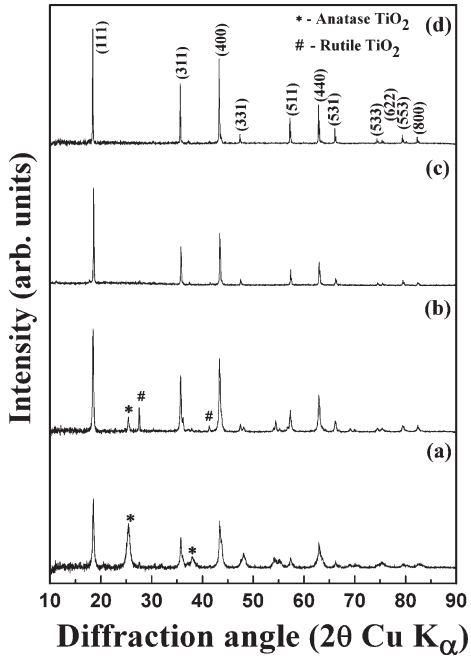

Figure 2. Powder XRD patterns for the products formed by the combustion of lithium and titanium nitrates with glycine at (a) 500 °C, (b) 700 °C, (c) 800 °C, and (d) $Li_4Ti_5O_{12}$ prepared by solid-state method.

formed at 700 °C (Figure 2(b)) indicates the formation of $Li_4Ti_5O_{12}$ as the major phase with small amounts of anatase and rutile TiO_2 as impurities. The XRD pattern of the combustion product formed at 800 °C (Figure 2(c)) corresponds to pure $Li_4Ti_5O_{12}$ without any impurity phases and the pattern could be indexed in spinel structure with the *Fd*3*m* space group. The lattice parameter "*a*" for $Li_4Ti_5O_{12}$ calculated using a powder cell program is 8.361 Å, which agrees well with the literature.[4] The average crystallite size obtained using the Scherrer equation is 80 nm. The XRD pattern for the sample prepared by the solid-state reaction with the lattice parameter (*a*) = 8.357 Å is also shown in Figure 2(d) for comparison.

Figure 3(a−e) depicts the microstructure of combustion-derived LTO at different magnifications. As seen from the micrographs, the aggregates are flaky and highly porous in nature (Figure 3(a,b)). The porous structure is obtained because of concomitant formation of material with vigorous evolution of large volume of gases during the combustion reaction. The pore sizes vary between a few nano meters to a few micrometers but typically are between 150 nm to 1.5 μm (Figure 3(c−f)). The high magnification-image shown in Figure 3(f) indicates a unique architecture containing agglomeration of smaller particles of size < 150 nm with embedded nano and micro pores.

Transmission electron microscopy studies were also performed on LTO synthesized at 800 °C (LTO-800), and the bright field images at two different magnifications are shown in Figure 4(a,b). The micrographs show agglomeration of well crystallized nanoparticles of LTO with sizes ranging between 20 and 50 nm. This agrees well with the crystallite size calculated from XRD peak broadening using the Scherrer equation. All the particles have

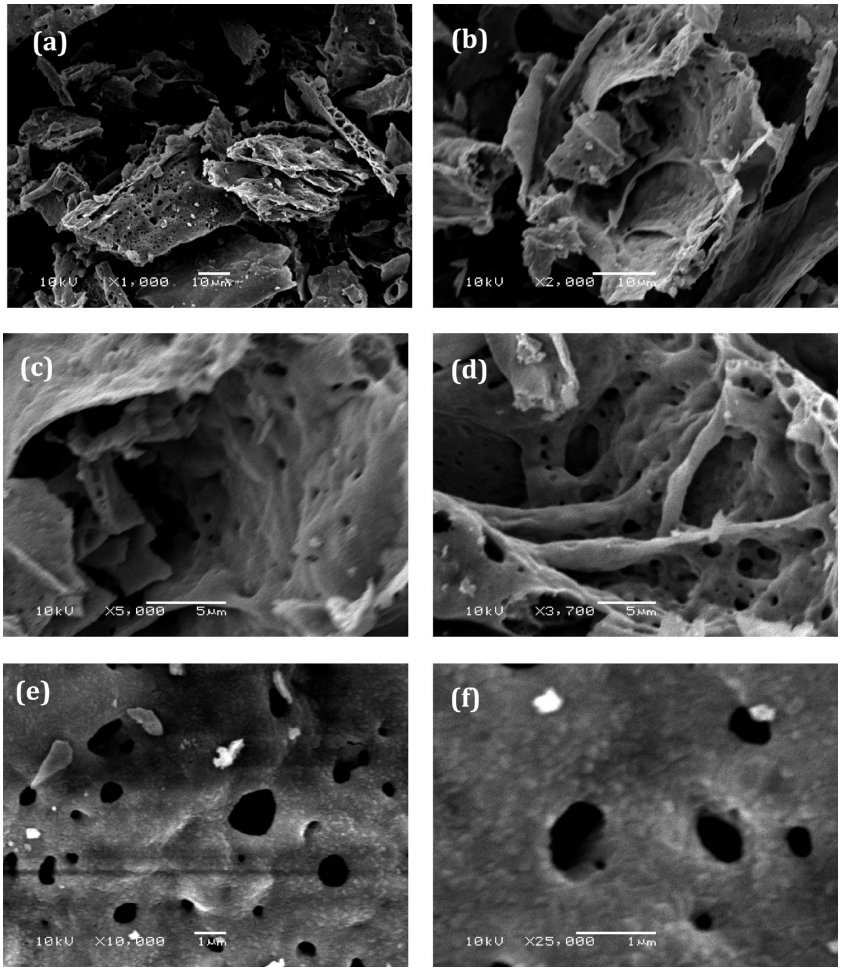

Figure 3. Scanning electron micrographs for nanocrystalline $Li_4Ti_5O_{12}$ at different magnifications synthesized by combustion method.

similar contrast indicating the absence of impurities like lithium salts or carbon. The irregular pore structures created by the fusion of agglomerates are seen in the micrographs. The selected area electron diffraction (SAED) pattern for an individual crystallite (Figure 4(b) inset) exhibits a single crystal-like spot pattern. The average-electron-diffraction pattern for $Li_4Ti_5O_{12}$ is shown in Figure 4(c), and the line profile deduced from electron diffraction is shown in Figure 4(d). The electron-diffraction pattern exhibits sharp spots suggesting a highly crystalline sample. The line profile of electron diffraction matches well that for $Li_4Ti_5O_{12}$ (JCPDS No: 00-049-0207) and confirms the phase purity at trace levels.

The voltage versus composition curves for LTO/Li cell cycled galvanostatically at C/2 (1 Li in 2 h) rate in the potential window between 2.0 and 1.2 V are shown in Figure 5(c). The cycling behavior is typical of LTO with a flat plateau at an average potential of 1.55 V which is attributed to a two-phase phenomenon pertaining to $Li_4Ti_5O_{12}$ and $Li_7Ti_5O_{12}$ phases.[32−36] The topotactic insertion/deinsertion of lithium in $Li_4Ti_5O_{12}$ and $Li_7Ti_5O_{12}$ phases during charge/discharge processes is depicted schematically in Figure 5, panels (a) and (b), respectively. The cation distribution in $Li_4Ti_5O_{12}$ and $Li_7Ti_5O_{12}$ phases during electrochemical charge/discharge processes could be written as follows:

$$[Li]_{8a}[Li_{1/3}Ti_{5/3}]_{16d}[O_4]_{32e} + Li^+ + e - \leftrightarrow [Li_2]_{16c}[Li_{1/3}Ti_{5/3}]_{16d}[O_4]_{32e}$$

During the first discharge $Li_4Ti_5O_{12}$ takes about 2.92 Li atoms corresponding to a capacity of 170 mA h/g that matches well with the expected theoretical capacity for $Li_4Ti_5O_{12}$. Although a small irreversibility of about 5% is observed in the subsequent charge cycles, the overall capacity after the first cycle remains almost unchanged at 162 mA h/g for several cycles. A small electrode polarization of about 0.02 V is observed between charge−discharge curves indicating the existence of good interparticle electrical contacts and better ion transport owing

(32) Murphy, D. W.; Greenblatt, M.; Zahurak, S. M.; Cava, R. J.; Waszczak, J. V.; Hull, G. W.; Hutton, R. S. *Rev. Chim. Miner.* **1982**, *19*, 441.
(33) Murphy, D. W.; Cava, R. J.; Zahurak, S. M.; Santoro, A. *Solid State Ionics* **1983**, *9&10*, 413.
(34) Wagemaker, M.; Simon, D. R.; Kelder, E. M.; Schoonman, J.; Ringpfeil, C.; Haake, U.; Lützenkirchen-Hecht, D.; Frahm., R.; Mulder, F. M. *Adv. Mater.* **2006**, *18*, 3169.
(35) Wagemaker, M.; Van Eck, E. R. H.; Kentgens, A. P. M.; Mulder, F. M. *J. Phy. Chem. B.* **2009**, *113*, 224.
(36) Kanamura, K.; Umegaki, T.; Naito, H.; Takehara, Z.; Yao, T. *J. Appl. Electrochem.* **2001**, *31*, 73.

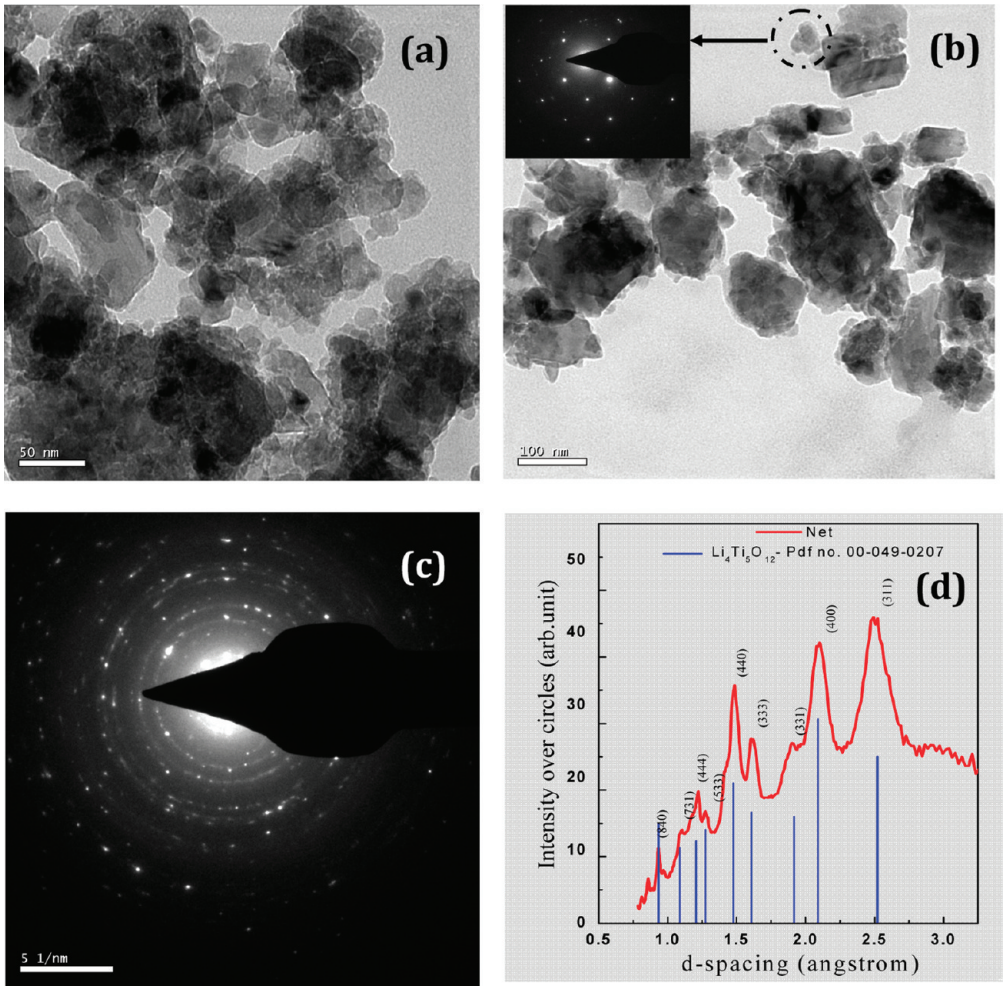

Figure 4. (a, b) Transmission electron micrographs for $Li_4Ti_5O_{12}$, (c) electron diffraction pattern, and (d) line profile of electron diffraction.

to the high degree of porosity of our combustion-made powders.

Nanocrystalline $Li_4Ti_5O_{12}$ is subjected to cycling at different charge−discharge rates to evaluate capacity-rate relationship, and the results are compared with the bulk sample prepared by solid-state synthesis. Figure 6 shows the voltage versus capacity plot for nanocrystalline $Li_4Ti_5O_{12}$ at several charge−discharge rates in the voltage range between 2.0 and 1 V. It is noteworthy that the current density during each charge and discharge is kept the same for all the experiments. At 0.5 C charge−discharge, the LTO-800 sample exhibits a capacity value of 170 mA h/g, a value close to the theoretical value of 175 mA h/g. The capacity values at 1C, 5C, and 10C rates are found to be 158, 147, and 140 mA h/g, respectively, with closely placed voltage plateaus below 10C, indicating that the crystallite size has only a minor effect on the rate capability of LTO below 10C. At charge−discharge rates >10 C, there is a considerable drop in capacity values together with a drop in discharge voltage plateau which cause high electrode polarization. Both of these are associated to the sluggish Li-ion diffusion kinetics at very high rates. However, a capacity of 125, 102, 90, and 70 mA h/g is obtained for 25, 50, 80, and 100C rates, respectively. These capacity values are higher than those reported in the literature for nanosized LTO at similar rates[20,21,37,38] (electrode surface $=1$ cm^2; active-material loading $=4$ mg/cm^2). These values are by far quite higher than those exhibited by bulk samples prepared by solid-state reaction (inset to Figure.6). It is noteworthy that the capacity (105 mA h/g) obtained with nanosized LTO at the 50C rate is higher than that obtained at the 5C rate (95 mA h/g) with bulk LTO. This is most likely nested in the morphology of our mesoporous powders made of fused nanoparticles with the nanoparticles providing a short diffusion path for Li and the pores fill of electrolytes ensuring a high flux of Li. However, too much porosity can result in a low volumetric energy density.

Figure 7 show plots of capacity as a function of cycle numbers for combustion derived and solid-state prepared samples (shown as inset) in the voltage window between 2.0 and 1.0 V at different charge−discharge rates. As can be seen from these data, combustion-derived LTO shows excellent capacity retention irrespective of the rate used. Interestingly, more than 95% capacity is retained even after 100 cycles. A solid-state synthesized compound also

(37) Huang, J.; Jiang, Z. *Electro. Chem. Acta* **2008**, *53*, 7756.
(38) Tang, Y.; Yang, L.; Qiu, Z.; Huang, J. *J. Mater. Chem.* **2009**, *19*, 5980.

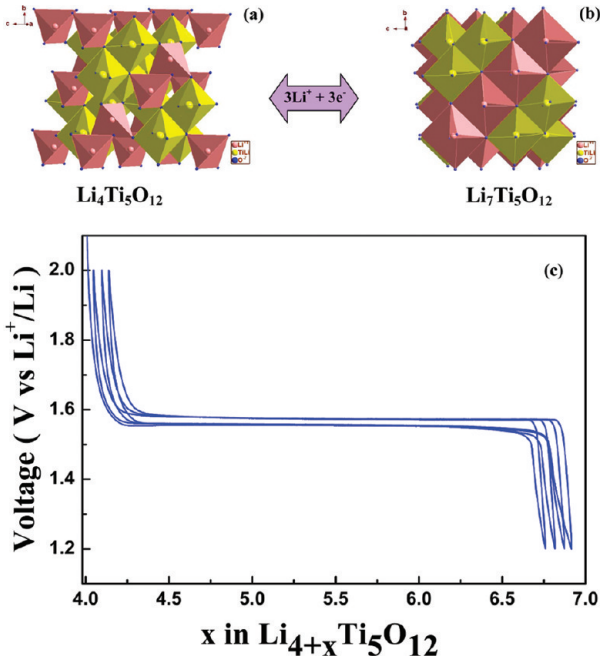

Figure 5. Structure of (a) spinel $Li_4Ti_5O_{12}$ and (b) ordered rocksalt-phase $Li_7Ti_5O_{12}$; (c) voltage-composition curves showing the electrochemical transformation of $Li_4Ti_5O_{12}$–$Li_7Ti_5O_{12}$ during galvanostatic charge–discharge cycles at C/2 rate at 30 °C.

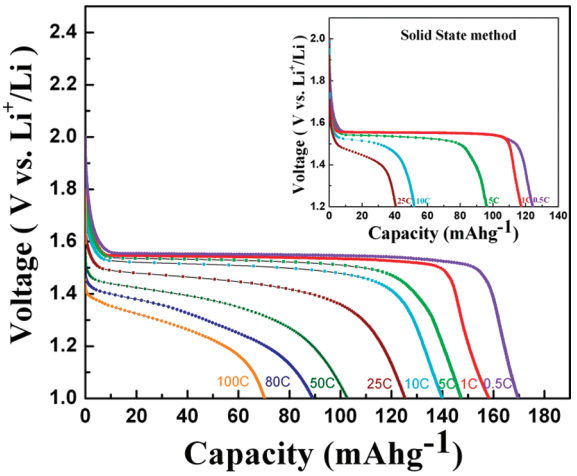

Figure 6. Capacity-voltage profile for nanocrystalline $Li_4Ti_5O_{12}$ synthesized by the combustion method at different rates. Inset shows capacity voltage profile for bulk $Li_4Ti_5O_{12}$ prepared by the solid-state method.

exhibits good capacity-retention but with lower rate-capability.

Ragone plots are derived from constant power experiments by measuring the time for one complete charge/discharge. The plot shows higher specific-power and specific-energy values for the combustion-derived LTO/Li half cells in relation to that derived by the solid-state route (Figure 8). Specific-energy values for both the samples at 70 W/kg specific powers correspond to ~270 Wh/kg. At high specific-power of 5000W/kg, the combustion-derived sample exhibits a specific energy of 182 Wh/kg against only about 3Wh/kg for the solid-state sample. Even during 5 min of charge/discharge, the

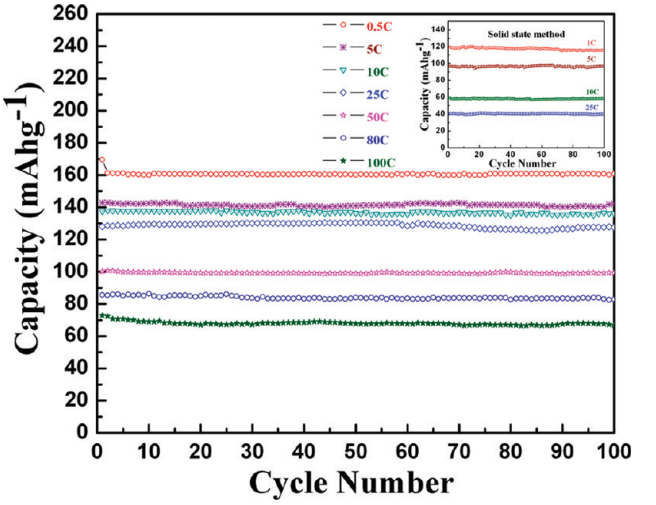

Figure 7. Capacity versus cycle number plot for nanocrystalline $Li_4Ti_5O_{12}$ synthesized by the combustion method at different discharge rates. Inset shows capacity versus cycle number for bulk $Li_4Ti_5O_{12}$.

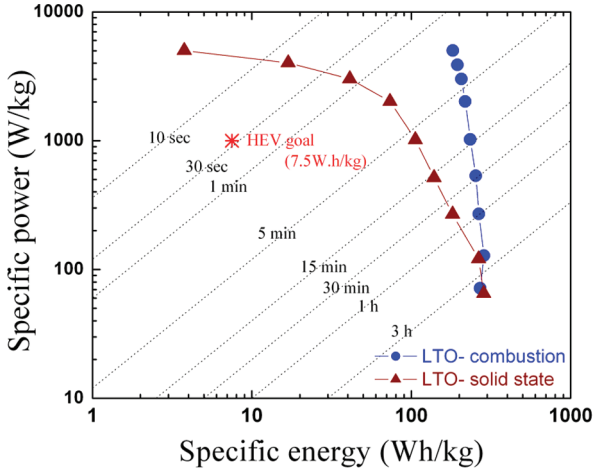

Figure 8. Ragone plot comparing the performance of $Li_4Ti_5O_{12}$ prepared by (-●-) combustion method and (-▲-) solid-state method when paired with metallic lithium; (*) DOE benchmark for HEVs.

combustion-derived material yields 167 A h/kg which is about 95% of the theoretical capacity as against 70 A h/kg for solid-state-derived samples which is only 40% of the theoretical capacity. It is seen from the data in Figure 8 that the specific-energy values for LTO/Li systems meet the HEV requirements.

Conclusions

Combustion synthesis is successfully used for the preparation of nanocrystalline $Li_4Ti_5O_{12}$ with particle size ranging between 20 and 50 nm with reaction times in the order of few minutes. A capacity value of 170 mA h/g is achieved at the 0.5C rate. At rates <10C, the observed capacity is closer to the theoretical value, and a value of 140 mA h/g is obtained at the 10C rate. Higher rates affect the moderate decrease in capacity with more than 40% of the theoretical capacity retained at 100C. Irrespective of rates used, nanocrystalline $Li_4Ti_5O_{12}$ retain their initial capacity up to 100 cycles. These results suggest that $Li_4Ti_5O_{12}$ prepared by the combustion technique is superior

in terms of both high rate-capability and capacity retention, which can be attributed to the presence of highly crystalline nanoparticles of $Li_4Ti_5O_{12}$ which agglomerate to form highly porous nanostructures having $\approx$12 m^2/g BET surface areas. Thus, combustion-derived $Li_4Ti_5O_{12}$ is an attractive anode material for high-power cathode lithium-ion batteries.

Acknowledgment. We gratefully acknowledge the financial support from the Council of Scientific and Industrial Research, New Delhi under EFYP.